ACS Catalysis

Research Article

pubs.acs.org/acscatalysis

Electrochemical CO_2 Reduction to Formic Acid at Low Overpotential and with High Faradaic Efficiency on Carbon-Supported Bimetallic Pd–Pt Nanoparticles

Ruud Kortlever, Ines Peters, Sander Koper, and Marc T. M. Koper*

Leiden Institute of Chemistry, Leiden University, P.O. Box 9502, 2300 RA Leiden, The Netherlands

Supporting Information

ABSTRACT: The electrochemical reduction of CO_2 has attracted significant interest recently, as it is a possible reaction for the storage of renewable energy. Here, we report on the synthesis of $Pd_xPt_{(100-x)}$/C nanoparticles and their electrocatalytic properties for the reduction of CO_2 to formic acid, compared with their activity for the reverse oxidation of formic acid to CO_2. We find that $Pd_xPt_{(100-x)}$/C nanoparticles have a very low onset potential for the reduction of CO_2 to formic acid of ca. 0 V vs RHE, which approaches the theoretical equilibrium potential of 0.02 V vs RHE for this reaction. Furthermore, the $Pd_{70}Pt_{30}$/C catalyst shows a faradaic efficiency of 88% toward formic acid after 1 h of electrolysis at −0.4 V vs RHE with an average current density of ∼5 mA/cm^2. Therefore, this catalyst shows a competing or even better faradaic efficiency toward formic acid compared to recently reported catalysts, at a substantially lower overpotential, while avoiding a strong deactivation that was observed with previously reported Pd-based catalysts.

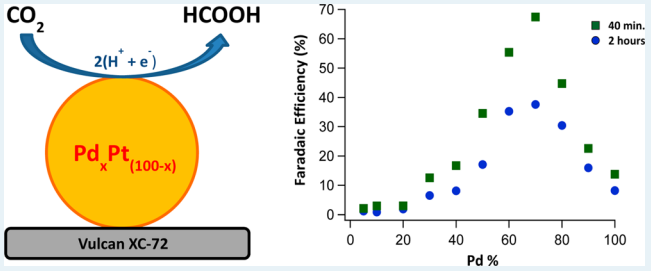

KEYWORDS: *electrocatalysis, CO_2 reduction, palladium–platinum catalysts, nanoparticles, formic acid*

1. INTRODUCTION

The electrochemical reduction of CO_2 has attracted a lot of attention in recent years since there is a need for a carbon-neutral energy carrier for the storage of renewable power.[1,2] By the production of fuels from CO_2 one could close the anthropogenic carbon cycle, which will not only have the advantage of an easy implementation into the existing fuel infrastructure, provided the fuel is a liquid, but could also have the advantage of lowering the possibly harmful CO_2 concentration in the atmosphere.

One of the possible products from electrocatalytic CO_2 reduction is formic acid. Since formic acid is used as fine chemical and can be used as a fuel in a direct formic acid fuel cell (DFAFC),[3] efficient production of formic acid from CO_2 is a very relevant process. Currently, most catalysts that have been reported to selectively make formic acid from CO_2 are poor metal-based catalysts such as Cd, Sn, Pb, and In.[4,5] The main issue with this class of catalysts is that in general they require very negative potentials to selectively produce formic acid, although recent advances have decreased the overpotential significantly.[6−8]

Recently, we reported the electrochemical reduction of CO_2 to formic acid on electrodeposited palladium layers on a platinum substrate with considerably lower overpotentials than previously reported catalysts.[9] This catalyst material was based on the idea that for a two-electron transfer reaction, such as the oxidation of formic acid, reversible catalysts must exist;[10] thus, catalysts that are very active for the electrochemical oxidation of formic acid should also be active for the reverse electrochemical reduction of CO_2 to formic acid. Since the best formic acid oxidation catalysts contain palladium and/or platinum,[11,12] a combination of these metals was chosen. It was shown that electrodeposited palladium layers on a platinum substrate (Pd–Pt) exhibit a significant decrease in the onset potential for formic acid production from CO_2 compared to bulk palladium; a decrease from −1.2 V vs RHE (for bulk palladium) to −0.1 V vs RHE (for Pd–Pt) was observed. An accompanying advantage of the Pd–Pt catalyst was that since the electrode was already shown to be active for formic acid oxidation, reversible reduction of CO_2 and oxidation of formic acid is possible on this material. Although Pd–Pt was shown to be able to produce formic acid from CO_2 almost selectively at low overpotentials, it was observed that the reduction of CO_2 and oxidation of formic acid on Pd–Pt was rapidly poisoned by the formation of CO on the surface of the catalyst, thereby quickly diminishing the catalytic activity.[9,13]

In an effort to overcome this problem and to develop an electrocatalyst with low overpotential, high faradaic efficiency, and high stability, we will here explore the possibilities of PdPt/C nanoparticles with different palladium to platinum ratios for both the reduction of CO_2 and the oxidation of formic acid. Since the oxidation of formic acid on PdPt nanoparticles has already been studied extensively,[14−16] we will use the systematic

Received: March 20, 2015
Published: May 15, 2015

DOI: 10.1021/acscatal.5b00602
ACS Catal. 2015, 5, 3916−3923

study of formic acid oxidation on PdPt nanoalloys by Cai et al.[16] as a guideline. The optimal Pd−Pt ratio for the reduction of CO_2 will be studied, including their corresponding faradaic efficiency, and compared to the optimal ratio for formic acid oxidation.

2. EXPERIMENTAL SECTION

2.1. Materials. Cylindrical highly ordered pyrolitic graphite electrodes (HOPG), purchased at GE Quartz Europe GmbH, with a diameter of 5 mm and 10 mm connected to platinum wire were used as working electrodes. Prior to every experiment, the working electrodes were polished mechanically to a mirrorlike finish using P2500 sandpaper. After this, the electrodes were sonicated in ultrapure water.

Electrolytes were made from ultrapure water (Millipore Milli-Q gradient A10 system, 18 mΩ cm) and high-purity reagents (Merck Suprapur, Sigma-Aldrich TraceSelect). Before each experiment, the electrolytes were first purged with argon (Air Products, 5.7) for 15 min to remove air from the solution. In the case of CO_2 reduction experiments, the electrolyte was subsequently purged with CO_2 (Linde, 4.5) for at least 30 min to saturate the solution.

2.2. Preparation of $Pd_xPt_{(100-x)}$/C Nanoparticles. The procedure followed for the synthesis was similar to the one reported by Cai et al.[16] However, we extended this method to also make platinum-enriched nanoparticles. As was reported by Cai et al., this method is not particularly suitable for the synthesis of Pt/C nanoparticles. Since nanoparticles with high Pt content showed poor electrocatalytic properties compared to Pd-rich nanoparticle, Pt/C nanoparticles were not included in this study. Stock solutions of 0.05 M K_2PdCl_4, 0.05 M K_2PtCl_4, and 0.1 M ethylenediaminetetraacetic acid (EDTA) were made and added in the appropriate amounts (see Table S1) to 26 mL of ultrapure water in a 100 mL round-bottom flask. The flask was heated to 60 °C and kept at this temperature for 40 min under vigorous stirring. After 40 min, the solution was allowed to cool to room temperature, and the pH of the solution was adjusted to ca. 9−10 with a 0.3 M NaOH solution. Afterward, 32 mg of Vulcan XC-72 (Cabot Corporation) was added as carbon support, and this suspension was sonicated for 30 min. Next, 6 mL of 0.05 M Na_2CO_3 solution containing 18 mg of $NaBH_4$ was added dropwise over the course of 20 min. After this addition, the mixture was stirred at room temperature for 2 h. The nanoparticles were collected by centrifugation at 4500 rpm for 20 min and were washed three times with ultrapure water.

After synthesis, the nanoparticles were dried in air and analyzed with X-ray powder diffraction, inductively coupled plasma optical emission spectroscopy (ICP-OES), and transmission electron microscopy (TEM). X-ray powder diffraction analysis was performed on a Philips X'pert diffractometer, equipped with an X'celerator, using Cu Kα radiation. The data were recorded in the 2θ range between 10° and 100°. For ICP-OES, nanoparticle samples were first allowed to dissolve in aqua regia (3:1 HCl/HNO_3) for at least 48 h. The samples were then filtered and analyzed with a Varian Vista-MPX CCD Simultaneous ICP-OES. TEM images were obtained with a JEOL TEM 1010.

2.3. Electrochemical Measurements. Cyclic voltammetry measurements were carried out in a standard electrochemical cell using a three-electrode assembly at room temperature. The cell and all other glassware were first cleaned by boiling in a 1:1 mixture of concentrated sulfuric and nitric acid and were cleaned before every experiment by boiling in ultrapure water. A highly ordered pyrolitic graphite electrode with a diameter of 5 mm was used as the working electrode on which 10 μL of a 5 wt % Nafion solution containing approximately 10 mg/mL of PdPt/C nanoparticles was dropcasted. A coiled gold wire was used as counter electrode. All potentials are reported versus the reversible hydrogen electrode (RHE) as a reference electrode in a separate compartment filled with the same electrolyte, at the same pH as the electrolyte in the electrochemical cell. The voltammograms were recorded on an Ivium A06075 potentiostat at a scan rate of 50 mV s^{-1}.

Faradaic efficiency measurements were carried out in a custom-made H-type cell with a cathodic and an anodic compartment separated by a Nafion 115 membrane (see Figure S6, Supporting Information). The cell was cleaned in a similar way as the cell used for cyclic voltammetry. A highly ordered pyrolitic graphite electrode with a diameter of 10 mm was used as working electrode on which 50 μL of a 5 wt % Nafion solution containing approximately 10 mg/mL of $Pd_xPt_{(1-x)}$/C nanoparticles was dropcasted. A platinum flag electrode was used as counter electrode, and a Ag/AgCl reference electrode was used. The resistance of the cell was determined before every experiment by electrochemical impedance spectroscopy (EIS) on an Ivium A06075 potentiostat. For the chronoamperometry measurements, an Autolab PGSTAT101 potentiostat was used, which compensated for the ohmic drop that was measured with EIS. After the measurements, the applied potential was further corrected, if necessary, to give the real electrode potential vs RHE.

2.4. Detection and Quantification of Products. For online detection of products dissolved in the electrolyte as a function of applied potential online high-performance liquid chromatography (HPLC) was used.[17] While the potential was being changed from 0.0 V to the required potential, samples were collected with an open tip positioned close (∼10 μm) to the electrode. Sampling was done at a rate of 60 μL min^{-1}, and each sample had a volume of 60 μL. Since the potential was changed at 1 mV s^{-1}, each sample contained the products averaged over a potential change of 60 mV. After voltammetry, these samples were analyzed by HPLC (Prominence HPLC, Shimadzu; Aminex HPX 87-H column, Biorad). Faradaic efficiencies were determined by analyzing 100 μL aliquots of the electrolyte, which were taken every 10 min during electrolysis, with HPLC.

3. RESULTS AND DISCUSSION

3.1. Characterization. The as-synthesized nanoparticles were characterized with X-ray diffraction and ICP-OES (see Figure S1 and Table 1). The composition of the nanoparticles could be controlled very well with the method that was used, since the maximum deviation in the composition from the targeted $Pd_xPt_{(100-x)}$ composition was 1.5%. In contrast, the loading of the nanoparticles was more difficult to control. In the synthesis, we aimed at a loading of 20 wt % $Pd_xPt_{(100-x)}$ on Vulcan XC-72; the actual loading, however, varies between 11.8 wt % (for $Pd_{90}Pt_{10}$/C) and 33.7 wt % (for Pd_5Pt_{95}/C). The loading of the nanoparticles does not influence the electrocatalytic properties greatly, since no significant electrocatalytic

Table 1. Actual Compositions of the Synthesized $Pt_xPd_{(100-x)}$/C Nanoparticles and Their Corresponding Loading on Vulcan XC-72 As Measured with ICP-OES and Their Average Size As Measured with XRD and Calculated with the Scherrer Equation

calcd composition	measured composition	loading (wt %)	particle size (nm)
Pd_5Pt_{95}/C	$Pd_{4.5}Pt_{95.5}$/C	33.7	4.4
$Pd_{10}Pt_{90}$/C	$Pd_{11.5}Pt_{88.5}$/C	24.4	3.8
$Pd_{20}Pt_{80}$/C	$Pd_{20.9}Pt_{79.1}$/C	21.4	4.1
$Pd_{30}Pt_{70}$/C	$Pd_{29.5}Pt_{70.5}$/C	17.2	4.1
$Pd_{40}Pt_{60}$/C	$Pd_{39.3}Pt_{60.7}$/C	32.3	3.8
$Pd_{50}Pt_{50}$/C	$Pd_{49.6}Pt_{50.4}$/C	16.5	4.0
$Pd_{60}Pt_{40}$/C	$Pd_{59.7}Pt_{40.3}$/C	15.6	3.7
$Pd_{70}Pt_{30}$/C	$Pd_{70.9}Pt_{29.1}$/C	20.1	4.3
$Pd_{80}Pt_{20}$/C	$Pd_{78.8}Pt_{21.2}$/C	16.4	4.2
$Pd_{90}Pt_{10}$/C	$Pd_{88.6}Pt_{11.4}$/C	11.8	4.2
$Pd_{95}Pt_5$/C	$Pd_{94.1}Pt_{5.9}$/C	14.8	4.1
Pd/C	Pd/C	12.0	3.1

DOI: 10.1021/acscatal.5b00602
ACS Catal. 2015, 5, 3916−3923

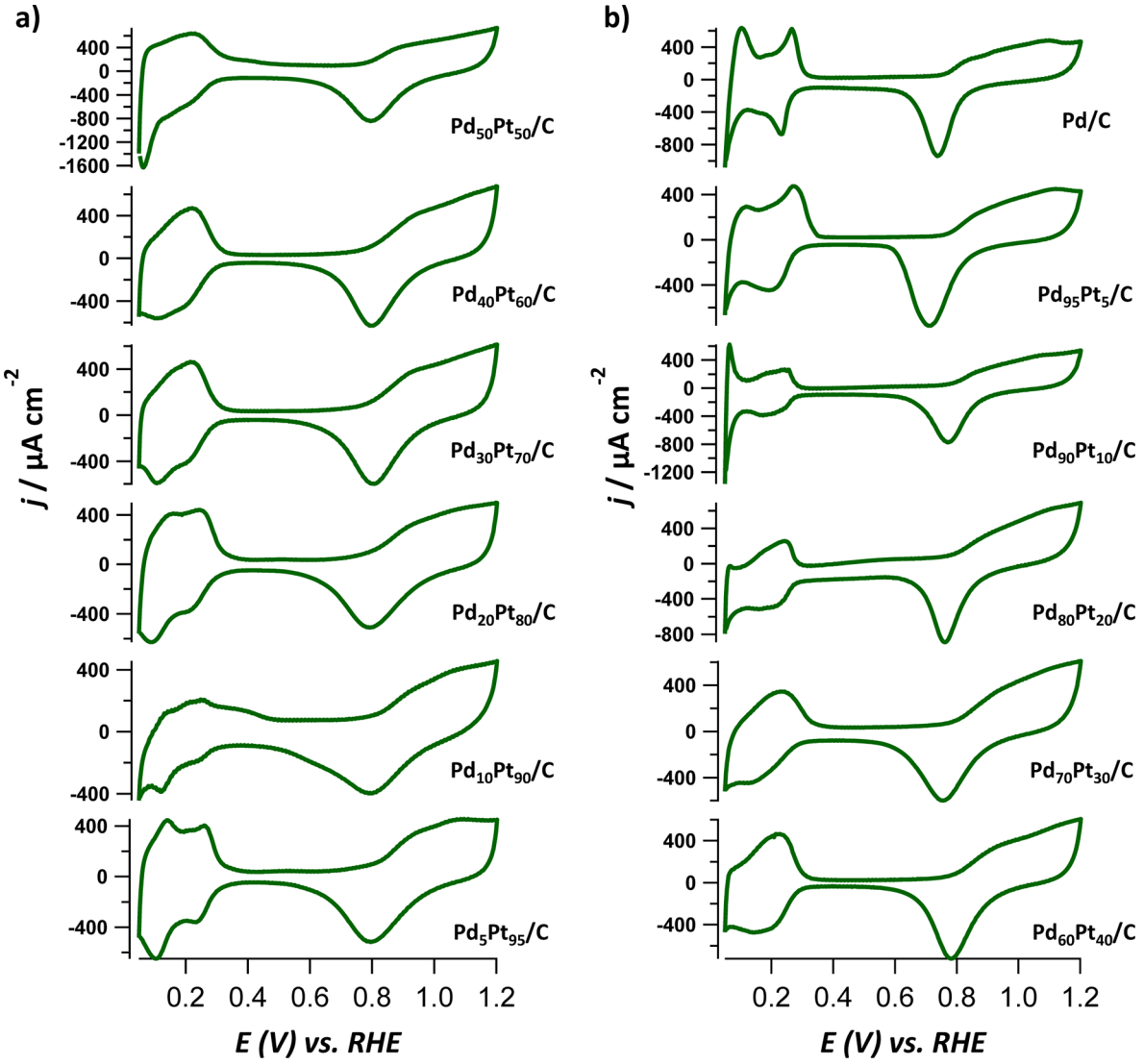

Figure 1. Cyclic voltammograms of the synthesized $Pd_xPt_{(100-x)}/C$ nanoparticles in a 0.5 M H_2SO_4 solution at a scan rate of 20 mV/s: (a) cyclic voltammograms of Pd_5Pt_{95}/C, $Pd_{10}Pt_{90}/C$, $Pd_{20}Pt_{80}/C$, $Pd_{30}Pt_{70}/C$, $Pd_{40}Pt_{60}/C$, and $Pd_{50}Pt_{50}/C$; (b) cyclic voltammograms of $Pd_{60}Pt_{40}/C$, $Pd_{70}Pt_{30}/C$, $Pd_{80}Pt_{20}/C$, $Pd_{90}Pt_{10}/C$, $Pd_{95}Pt_5/C$, and Pd/C.

differences were observed between batches of the same $Pd_xPt_{(100-x)}/C$ composition with different loading (see Figure S2).

The X-ray diffraction spectra show a first peak around 25° which is ascribed to the amorphous carbon support, and characteristic peaks for face-centered-cubic (fcc) crystalline Pd and Pt, corresponding to the (111), (200), (220), and (311) planes, respectively. Especially in the peak corresponding to the (111) plane, a small shift to lower 2θ values is seen with increasing ratio of Pt in the alloy nanoparticles. This shift is caused by a lattice expansion due to the incorporation of larger Pt atoms in the Pd lattice.[18] The (111) peak in the X-ray diffraction spectra was used to calculate the average size of the $Pd_xPt_{(100-x)}/C$ nanoparticles with the aid of the Scherrer equation. The calculated average size for all bimetallic nanoparticles is around 4 nm; only the pure palladium nanoparticles deviate with a smaller average size of 3.1 nm. TEM images of the nanoparticles (see Figures S8 and S9) show that the distribution of the nanoparticles over the Vulcan XC-72 support is fairly even and that there is no large deviation in the size of the particles. Particle size distribution histograms corresponding to the TEM images show approximately the same average sizes for the nanoparticle samples as the average sizes calculated with the Scherrer equation (see Figures S10 and S11).

The nanoparticles were further characterized electrochemically by performing cyclic voltammetry in a 0.5 M H_2SO_4 electrolyte (Figure 1). In Figure 1b a clear shift in the cathodic peak potential for the stripping of oxides is seen as a function of nanoparticle composition. A negative shift of the oxide stripping peak potential is seen with increasing ratios of palladium, in agreement with previous studies.[16] To evaluate the effect of the changing ratio of Pd and Pt in the nanoparticles on the hydrogen adsorption and desorption region of the voltammograms, a lower potential boundary was chosen in such a way that hydrogen evolution and oxidation was excluded as much as possible. In the hydrogen adsorption and desorption region a shift was seen in both the hydrogen adsorption and hydrogen desorption peak potential. The peak potential shifted from 0.22 V vs RHE for $Pd_{50}Pt_{50}/C$ to 0.27 V vs RHE for Pd/C for the hydrogen adsorption, while for

DOI: 10.1021/acscatal.5b00602
ACS Catal. 2015, 5, 3916−3923

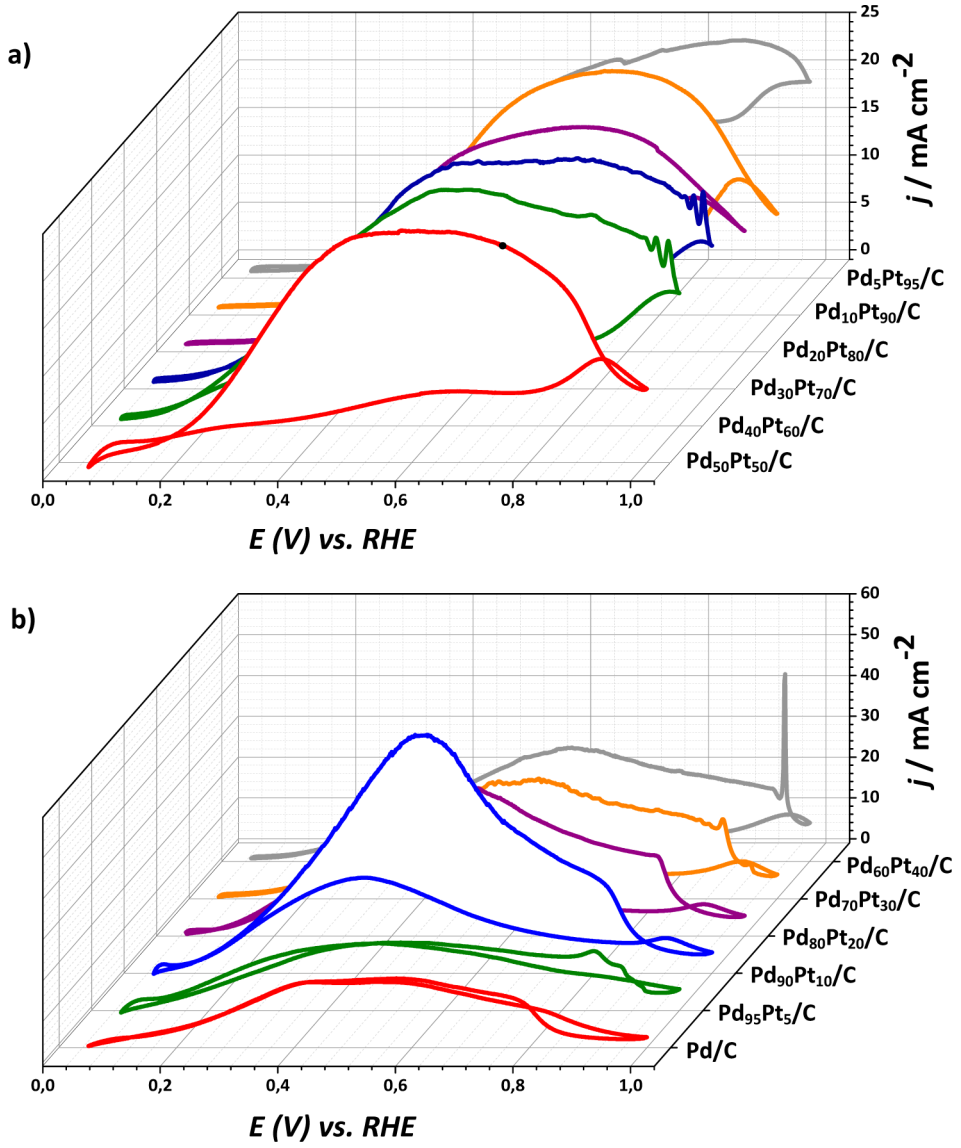

Figure 2. Cyclic voltammograms recorded of $Pd_xPt_{(100-x)}$/C nanoparticles in a 0.5 M H_2SO_4 electrolyte containing 0.5 M formic acid at a scan rate of 20 mV/s: (a) cyclic voltammograms of Pd_5Pt_{95}/C (gray), $Pd_{10}Pt_{90}$/C (orange), $Pd_{20}Pt_{80}$/C (purple), $Pd_{30}Pt_{70}$/C (blue), $Pd_{40}Pt_{60}$/C (green), and $Pd_{50}Pt_{50}$/C (red); (b) cyclic voltammograms of $Pd_{60}Pt_{40}$/C (gray), $Pd_{70}Pt_{30}$/C (orange), $Pd_{80}Pt_{20}$/C (purple), $Pd_{90}Pt_{10}$/C (blue), $Pd_{95}Pt_5$/C (green), and Pd/C (red).

hydrogen desorption the peak potential shifted from 0.12 V vs RHE for $Pd_{50}Pt_{50}$/C to 0.23 V vs RHE for Pd/C.

In Figure 1a, voltammograms are shown for nanoparticles ranging from $Pd_{50}Pt_{50}$/C to Pd_5Pt_{95}/C. In these voltammograms, no shift of the oxide stripping peak is observed. However, it can be clearly seen that as the amount of Pt is increased in the nanoparticles the behavior of the nanoparticles in the hydrogen adsorption and desorption region shifts to more Pt-like behavior, eventually evolving the two distinctive hydrogen adsorption and desorption peaks for Pd_5Pt_{95}/C.

3.2. Formic Acid Oxidation on $Pd_xPt_{(100-x)}$/C Nanoparticles. The electro-oxidation of formic acid on the synthesized $Pd_xPt_{(100-x)}$/C nanoparticles was studied in an electrolyte containing 0.5 M H_2SO_4 and 0.5 M formic acid, and cyclic voltammograms with a scan rate of 20 mV/s from 0.05 to 1.0 V vs RHE were recorded (see Figure 2a,b). For the nanoparticles with compositions from Pd_5Pt_{95}/C to $Pd_{50}Pt_{50}$/C, similar current densities are measured for the oxidation of formic acid (see Figure 2a). The measured current was always smaller in the forward going scan than in the back scan. A shift in the peak potential is seen for these nanoparticles, with a peak potential of 0.9 V vs RHE for Pd_5Pt_{95}/C going to a peak potential between 0.5 and 0.6 V vs RHE for $Pd_{50}Pt_{50}$/C.

In Figure 2b, the cyclic voltammograms for nanoparticles with compositions from $Pd_{50}Pt_{50}$/C to Pd/C are shown. With an increasing amount of Pd a sharp peak in the measured current density starts to develop. Whereas $Pd_{50}Pt_{50}$/C gave a voltammogram with a broad peak for the oxidation of formic acid, $Pd_{90}Pt_{10}$ gives a sharp peak with a peak potential of 0.5 V vs RHE. In accordance with previous reports, the highest current densities are achieved with a composition of $Pd_{90}Pt_{10}$/C, both nanoparticles with higher and lower Pd ratios give lower current responses than $Pd_{90}Pt_{10}$/C.[15,16] Interestingly, in our experiments the peak current density for the oxidation of formic acid shifts to lower potentials with an increasing ratio of Pd in the nanoparticles. This observation does not agree with

DOI: 10.1021/acscatal.5b00602
ACS Catal. 2015, 5, 3916−3923

the results of Cai et al., since they reported the opposite trend for these nanoparticles with $Pd_{50}Pt_{50}/C$ giving a peak at the lowest potential.[16] Comparing our voltammograms with other literature studies, we find that our voltammogram for $Pd_{50}Pt_{50}/C$ is very comparable to the results of Hsing et al.,[15] where a similar broad oxidation peak is seen that peaks between 0.5 and 0.6 V vs RHE.

The electrochemical behavior of formic acid oxidation on the $Pd_xPt_{(100-x)}/C$ nanoparticles is explained by the hypothesis that in the forward going scan the surface is blocked by adsorbed CO that is formed from the dehydration of formic acid.[19] Once the potential increases, the adsorbed CO is stripped from the surface giving rise to a peak in the forward scan. The peak potential of this stripping of CO from the surface is dependent on the composition of the nanoparticles. Since the surface sites that were previously blocked by CO are now available to participate in the oxidation of formic acid, the current starts to increase reaching a peak around 0.8−0.9 V vs RHE. At this potential, the surface of the nanoparticles starts to oxidize, thus diminishing the activity toward formic acid oxidation. In the back scan, the surface oxide is stripped off the surface, leading to an increasing formic acid oxidation current. The current peak in the back scan is a consequence of the potential dependent formic acid oxidation and the renewed blocking of the surface by adsorbed CO, which cannot be stripped off at these low potentials.

Since the dehydration of formic acid to form CO is believed to take place on at least two neighboring Pt sites (called the "ensemble effect"),[20] an increase in the amount of Pd can effectively reduce the number of these Pt ensembles, thereby decreasing the effect of CO poisoning. Furthermore, the mixing of Pd and Pt will lead to a shift in the d-band center values for the nanoparticles.[21] Since the d-band center values for Pt and Pd are −2.25 and −1.83 eV, respectively, according to DFT calculations,[22] the addition of Pt will lower the d-band center value. Thus, the d-band center values for the $Pd_xPt_{(100-x)}/C$ nanoparticles can be finely tuned, which has been hypothesized to have an additional beneficial effect on the formic acid oxidation.[16]

3.3. CO_2 Reduction on $Pd_xPt_{(100-x)}/C$ Nanoparticles. Blank cyclic voltammograms of the $Pd_xPt_{(100-x)}/C$ were recorded in a pH 6.7 phosphate buffer electrolyte that was purged with argon and are compared with cyclic voltammograms in the same electrolyte purged with CO_2 in Figure 3 and Figure S9. For all compositions of the $Pd_xPt_{(100-x)}$ nanoparticles a decrease in current is seen in the CO_2 scan in comparison with the blank scan, indicating that the nanoparticles have an interaction with CO_2. The particles with high Pd ratios show a bigger decrease in current between the blank and CO_2 voltammogram, with the exception of $Pd_{95}Pt_5/C$, indicating that those particles have a stronger interaction with CO_2 than the particles with high ratios of Pt. In the CO_2 scans of Pd/C and $Pd_{95}Pt_5/C$ a reduction wave between 0 and −0.7 V vs RHE is observed, similar to what has been seen on the Pd layers deposited on Pt (Pd−Pt)[9] and Pd electrodes.[23] This reduction current is ascribed to the either direct or indirect reduction of HCO_3^- to formate/formic acid. Since the pH near the electrode surface will increase as the potential is decreased, due to continuous hydrogen evolution,[24] HCO_3^- will be generated in situ from CO_2 near the electrode surface due to the equilibrium between HCO_3^- and CO_2. For CO_2 reduction on the Pd−Pt layer system,[9] we observed that the reduction peak disappeared after the first scan, indicating a fast poisoning

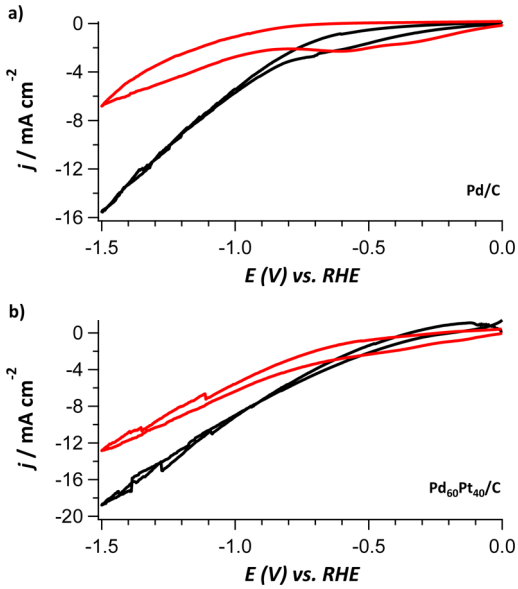

Figure 3. (a) Cyclic voltammograms of Pd/C nanoparticles recorded in a 0.1 M KH_2PO_4/0.1 M K_2HPO_4 electrolyte (pH 6.7) at a scan rate of 50 mV/s purged with either argon (black) or CO_2 (red). (b) Cyclic voltammograms of $Pd_{60}Pt_{40}/C$ nanoparticles recorded in a 0.1 M KH_2PO_4/0.1 M K_2HPO_4 electrolyte (pH 6.7) at a scan rate of 50 mV/s purged with either argon (black) or CO_2 (red).

by CO. For the Pd/C and $Pd_{95}Pt_5/C$ nanocatalysts studied here, the same observation was made, suggesting that CO poisoning for these nanoparticle compositions is fast as well.

The production of formic acid from CO_2 as a function of potential was followed with online HPLC (Figure 4). The production of formic acid is normalized to the total mass of nanoparticles that was dropcasted on the electrode. Except for Pd/C, all other $Pd_xPt_{(100-x)}/C$ nanoparticles had very comparable average sizes; thus, this normalization should give a fair comparison for the production of formic acid between the different nanoparticles. For all nanoparticle compositions, a peak in the production of formic acid is observed around −0.5 V vs RHE. The observation of this peak appears to be related to the presence of bicarbonate and has been observed on Pd−Pt layer systems as well.[9] However, on Pd−Pt layer electrodes production of formic acid was also observed at more negative potentials, starting form −0.9 V vs RHE, whereas the $Pd_xPt_{(100-x)}/C$ nanoparticles show no production of formic acid at these more negative potentials. The onset potential for formic acid production is around 0 V vs RHE for all of the nanoparticle compositions, which is the same for the Pd−Pt electrodes. This onset potential approaches the theoretical equilibrium potential of 0.02 V vs RHE for the production of formic acid from CO_2 in this electrolyte.

We note that nanoparticles with low ratios of Pd, up to $Pd_{20}Pt_{80}/C$ produce only small amounts of formic acid. With an increasing ratio of Pd in the nanoparticles, the production of formic acid grows, reaching a maximum at $Pd_{70}Pt_{30}/C$, while $Pd_{60}Pt_{40}/C$ and $Pd_{80}Pt_{20}/C$ also show a high production of formic acid. For nanoparticles with higher amounts of Pd, the production of formic acid decreases again.

Figure 5a shows the faradaic efficiencies for the production of formic acid on $Pd_xPt_{(100-x)}/C$ nanoparticles after a period of 40 min and 2 h at a potential of −0.5 V vs RHE. All the nanoparticle compositions show the production of formic acid over the course of 2 h. Remarkably, the $Pd_{95}Pt_5/C$ particles

DOI: 10.1021/acscatal.5b00602
ACS Catal. 2015, 5, 3916−3923

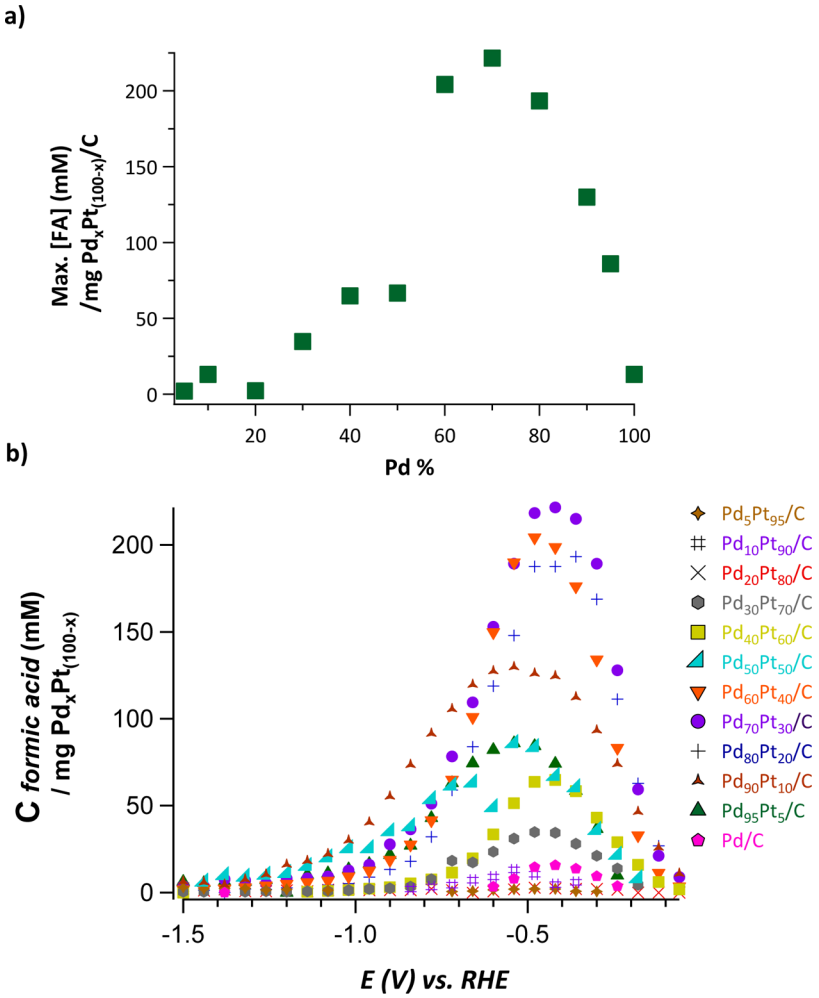

Figure 4. (a) Maximum concentration of formic acid that was observed with online HPLC, normalized by the mass of nanoparticles that was dropcasted on the electrode, as a function of the percentage of Pd in the nanoparticles. (b) Formation of formic acid as detected by online HPLC on $Pd_xPt_{(100-x)}/C$ nanoparticles in a 0.1 M K_2HPO_4/0.1 M KH_2PO_4 electrolyte.

consistently gave faradaic efficiencies that were a little higher than the trend observed in Figure 5a, for reasons that are not well understood; the faradaic efficiency data for this sample can be found in Table S3. We assume that besides formic acid hydrogen is produced as the major side product, similar to Pd−Pt,[9] which accounts for the remainder of the faradaic efficiency. The amount of gaseous CO that is produced as a side product at these potentials is assumed to be small, in correspondence to what has been observed for Pd and Pt electrodes.[25,26] We expect that the formation of strongly surface-bound CO may still play a role in the slow deactivation of the catalyst. However, as was also shown by Cai et al.[16] for formic acid oxidation, these PdPt nanocatalysts have been designed to show minimal CO poisoning, and we consider that this effect explains the considerably lower poisoning rate of these PdPt nanocatalysts in comparison with the Pd−Pt layer system studied in our previous paper.[9] Similar to the online HPLC experiments, only small amounts of formic acid are produced with nanoparticles with low amounts of Pd. The particles with a composition of $Pd_{20}Pt_{80}$ or with lower amounts of Pd show efficiencies between 2 and 3% toward formic acid. With increasing amount of Pd in the nanoparticles, an increase in the faradaic efficiency toward formic acid is observed, reaching an optimum at $Pd_{70}Pt_{30}/C$, similar to the results obtained with online HPLC. The $Pd_{70}Pt_{30}/C$ nanoparticles are able to convert CO_2 to formic acid with a maximum faradaic efficiency of 67%. For nanoparticles with a higher amount of Pd than $Pd_{70}Pt_{30}/C$ the faradaic efficiency toward formic acid decreases again. It should be noted, however, that the faradaic efficiency of the $Pd_{70}Pt_{30}/C$ nanoparticles, and also of the other nanoparticle compositions, is not constant and gradually decreases over time. For the $Pd_{70}Pt_{30}/C$ nanoparticles this means that at the end of the electrolysis experiments, after 2 h, the faradaic efficiency has dropped to 38%.

In an effort to avoid deactivation of the nanoparticles, the potential for the reduction of CO_2 to formic acid on the $Pd_{70}Pt_{30}/C$ nanoparticles was optimized (Figure 5b). A clear optimum in the applied potential was observed at −0.4 V vs RHE. At this potential, a maximum faradaic efficiency of 88% toward formic acid was achieved after 1 h of electrolysis. For potentials higher than −0.4 V vs RHE, the maximum faradaic efficiency decreases to 73%, 22%, and 21% for −0.3 V vs RHE, −0.2 V vs RHE, and −0.1 V vs RHE respectively. For all potentials, a deactivation was seen over the course of time. However, for −0.3, −0.2, and −0.1 V vs RHE the decrease in faradaic efficiency was less prominent, decreasing to 59%, 16%, and 17%, respectively, as compared to what was observed for

DOI: 10.1021/acscatal.5b00602
ACS Catal. 2015, 5, 3916−3923

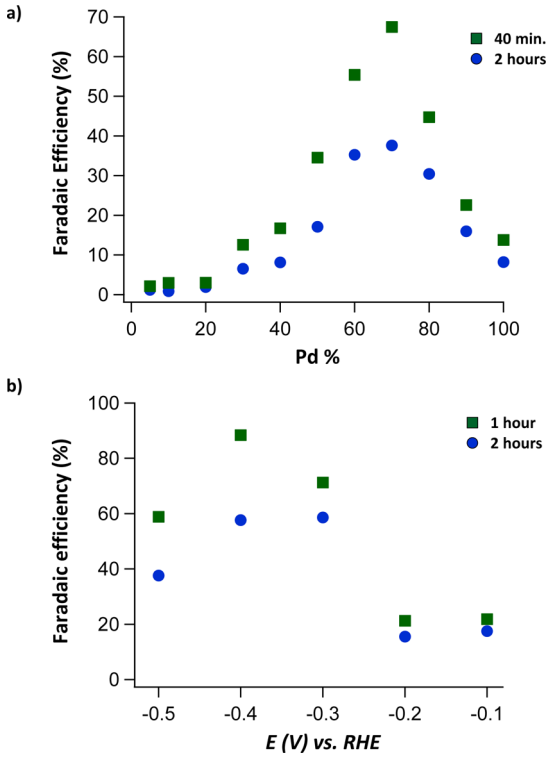

Figure 5. (a) Faradaic efficiencies toward the production of formic acid on $Pd_xPt_{(100-x)}$/C nanoparticles in a pH 6.7 phospate buffer (0.1 M KH_2PO_4/0.1 M K_2HPO_4) at −0.5 V vs RHE after 40 min (■) and after 2 h (●). (b) Faradaic efficiencies toward the production of formic acid on $Pd_{70}Pt_{30}$/C nanoparticles in a pH 6.7 phospate buffer (0.1 M KH_2PO_4/0.1 M K_2HPO_4) at different potentials after 1 h (■) and after 2 h (●).

−0.5 V vs RHE and −0.4 V vs RHE, at which potentials a decrease to 38% and 58%, respectively.

Pd-based catalysts have been previously reported to reduce CO_2 or bicarbonate to formic acid at low overpotentials.[9,13,27] Electrodeposited Pd layers on Pt have been shown to be able to produce formic acid almost selectively from CO_2 at potentials close to 0 V vs RHE.[9,13] However, since a fast poisoning effect diminishes the catalytic properties quickly, this material does not satify the requirements for an applicable catalyst. With the alloying of Pd with Pt we observe a drastic decrease in the poisoning rate, while the onset potential for the production of formic acid and the potential at which the production of formic acid peaks are not affected.

A $PdCl_4^{2-}$-impregnated polymer on a tungsten or platinum electrode has been shown to be able to reduce bicarbonate to formic acid with an efficiency of 85% at approximately −0.1 V vs RHE.[27] This efficiency however was achieved at a current density of 100 $\mu A/cm^2$ which decreased over the course of electrolysis to 50 $\mu A/cm^2$, while the authors state that "as the electrolyses proceed the more negative potentials required to sustain current flow are a consequence of the buildup of reduction product", indicating that long-term electrolysis at high current densities with this catalyst will seriously increase the overpotential that is necessary. Our catalyst is able to reduce CO_2 to formic acid at current densities that are almost 2 orders in magnitude higher. For the first 10 min of electrolysis with $Pd_{70}Pt_{30}$/C at −0.4 V vs RHE we observe a current density of approximately 7 mA/cm^2 which decreases to 3.5 mA/cm^2 after 2 h of electrolysis (see Figure S6). Therefore, the significant advance of this paper is that Pt is not only required to enhance the stability of the catalyst but also essential to achieve high faradaic efficiency at high current densities.

Compared to other catalysts reported in the recent literature, our best catalyst, $Pd_{70}Pt_{30}$/C, shows considerably lower onset potentials for the reduction of CO_2 to formic acid and correspondingly higher faradaic efficiencies toward formic acid at these low overpotentials. A Sn/SnO_x tin-film catalyst reported by Chen et al.[7] started producing formic acid at −0.5 V vs RHE and reached a maximum efficiency toward formic acid of 40% at −0.7 V vs RHE, with CO accounting for the remaining 60%. Zhang et al.[8] reported that the production of formic acid from CO_2 on nanostructured tin catalysts starts at −1.0 V vs SCE (−0.36 V vs RHE) and reached a maximum faradaic efficiency of 86.2% at −1.8 V vs SCE (−1.16 V vs RHE). A homogeneous iridium pincer complex in a gas diffusion electrode reported by Kang et al.[28] started producing formic acid at an onset potential of −1.0 V vs NHE (−0.6 V vs RHE) and achieved a faradaic efficiency of 96% at −1.2 V vs NHE (−0.8 V vs RHE) with a decreasing activity for higher potentials. Our catalyst thus achieves competing or better efficiencies toward formic acid at substantially lower overpotentials. Moreover, our catalyst also has a high activity for the reverse reaction, i.e., the oxidation of formic acid. This catalytic reversibility has not been demonstrated for the catalysts reported in the literature, other than for immobilized electroactive enzymes.[29]

The comparison between the composition sensitivity of formic acid oxidation and CO_2 reduction on the $Pd_xPt_{(100-x)}$/C nanoparticles shows a clear difference in optimal composition. Whereas the optimum composition for formic acid oxidation is $Pd_{90}Pt_{10}$/C, the optimal composition for CO_2 reduction is $Pd_{70}Pt_{30}$/C, with $Pd_{60}Pt_{40}$/C and $Pd_{80}Pd_{20}$/C also showing good efficiencies for the reduction of CO_2 to formic acid. Therefore, the ensemble effect and the breaking up of Pt ensembles must be less important for CO_2 reduction than for formic acid oxidation. We hypothesize that the fine-tuning of the d-band center by mixing Pt and Pd may also play a role in the enhancement of the catalytic activity. Futhermore, the addition of the bigger Pt atoms can induce lattice strain effects in the nanoparticles, which can have an additional beneficial effect.

4. CONCLUSIONS

In this paper, we have shown that $Pd_xPt_{(100-x)}$/C nanoparticles have a low onset potential for the production of formic acid from carbon dioxide, with formic acid production starting from 0 V vs RHE, very close to the theoretical equilibrium potential of 0.02 V vs RHE, in combination with very good selectivity. Depending on the composition of the nanoparticles, the faradaic efficiency toward formic acid can be very high, reaching a maximum of ca. 90% for the $Pd_{70}Pt_{30}$/C nanoparticles at an applied potential of −0.4 V vs RHE during 1 h of electrolysis. We show that this catalyst is able to avoid fast poisoning and is able to achieve good faradaic efficiencies at high current densities, which was problematic with earlier formulated Pd based catalysts. This catalyst is among the best catalysts to date with respect to the onset potential for the formation of formic acid and it is able to achieve higher or competing faradaic effiencies than other recently reported non Pd-based catalysts at substantially lower overpotential. Moreover, the catalyst obeys the reversibility principle in the sense that it also catalyzes the reverse reaction with a low overpotential.

DOI: 10.1021/acscatal.5b00602
ACS Catal. 2015, 5, 3916−3923

■ ASSOCIATED CONTENT

Supporting Information

The Supporting Information is available free of charge on the ACS Publications website at DOI: 10.1021/acscatal.5b00602.

Additional information on the synthesis and characterization of the $Pd_xPt_{(100-x)}/C$ nanoparticles, faradaic efficiency experiments, and voltammetric analysis of CO_2 reduction on the nanoparticles (PDF)

■ AUTHOR INFORMATION

Corresponding Author

*Fax: (+)31 071 527 4451. E-mail: m.koper@chem.leidenuniv.nl.

Notes

The authors declare no competing financial interest.

■ ACKNOWLEDGMENTS

This work is supported by NanoNextNL, a micro- and nanotechnology consortium of the Government of The Netherlands and 130 partners. We gratefully acknowledge the support of the Smart Mix Program of The Netherlands Ministry of Economic Affairs and The Netherlands Ministry of Education, Culture and Science. Jos van Brussel is kindly acknowledged for assisting with ICP-OES analysis, and Gerda Lamers is kindly acknowledged for assisting with TEM experiments.

■ REFERENCES

(1) Gattrell, M.; Gupta, N.; Co, A. *Energy Convers. Manage.* **2007**, *48*, 1255−1265.
(2) Whipple, D. T. K.; Kenis, P. J. A. *J. Phys. Chem. Lett.* **2010**, *1*, 3451−3458.
(3) Yu, X.; Pickup, P. G. *J. Power Sources* **2008**, *182*, 124−132.
(4) Hori, Y. In *Modern Aspects of Electrochemistry*; Vayenas, C., White, R. E., Gamboa-Aldeco, M. E., Eds.; Springer: New York, 2008; Vol. *42*, pp 89−189.
(5) Chaplin, R. P. S.; Wragg, A. A. *J. Appl. Electrochem.* **2003**, *33*, 1107−1123.
(6) Kwon, Y.; Lee, J. *Electrocatalysis* **2010**, *1*, 108−115.
(7) Chen, Y.; Kanan, M. W. *J. Am. Chem. Soc.* **2012**, *134*, 1986−1989.
(8) Zhang, S.; Kang, P.; Meyer, T. J. *J. Am. Chem. Soc.* **2014**, *136*, 1734−1737.
(9) Kortlever, R.; Balemans, C.; Kwon, Y.; Koper, M. T. M. *Catal. Today* **2015**, *244*, 58−62.
(10) Koper, M. T. M. *J. Electroanal. Chem.* **2011**, *660*, 254−260.
(11) Yu, X.; Pickup, P. G. *J. Appl. Electrochem.* **2011**, *41*, 589−597.
(12) Uhm, S.; Lee, H. J.; Lee, J. *Phys. Chem. Chem. Phys.* **2009**, *11*, 9326−9336.
(13) Podlovchenko, B. I.; Kolyadko, E. A.; Lu, S. *J. Electroanal. Chem.* **1994**, *373*, 185−187.
(14) Liu, B.; Li, H. Y.; Die, L.; Zhang, X. H.; Fan, Z.; Chen, J. H. *J. Power Sources* **2009**, *186*, 62−66.
(15) Li, X.; Hsing, M. *Electrochim. Acta* **2006**, *51*, 3477−3483.
(16) Zhang, H.-X.; Wang, C.; Wang, J.-X.; Zhai, J.-J.; Cai, W.-B. *J. Phys. Chem. C* **2010**, *114*, 6446−6451.
(17) Kwon, Y.; Koper, M. T. M. *Anal. Chem.* **2010**, *82*, 5420−5424.
(18) Wang, W.; Huang, Q.; Liu, J.; Zou, Z.; Li, Z.; Yang, H. *Electrochem. Commun.* **2008**, *10*, 1396−1399.
(19) Baranova, E. A.; Miles, N.; Mercier, P. H. J.; Le Page, Y.; Patarachao, B. *Electrochim. Acta* **2010**, *55*, 8182−8188.
(20) Park, S.; Xie, Y.; Weaver, M. J. *Langmuir* **2002**, *18*, 5792−5798.
(21) Greeley, J.; Nørskov, J. K.; Mavrikakis, M. *Annu. Rev. Phys. Chem.* **2002**, *53*, 319−348.
(22) Ruban, A.; Hammer, B.; Stoltze, P.; Skriver, H. L.; Nørskov, J. K. *J. Mol. Catal. A: Chem.* **1997**, *115*, 421−429.
(23) Spichiger-Ulmann, M.; Augustynski, J. *J. Chem. Soc., Faraday Trans. 1* **1985**, *81*, 713−716.
(24) Gupta, N.; Gattrell, M.; MacDougall, B. *J. Appl. Electrochem.* **2006**, *36*, 161−172.
(25) Kolbe, D.; Vielstich, W. *Electrochim. Acta* **1996**, *41*, 2457−2460.
(26) Hori, Y.; Wakebe, H.; Tsukamoto, T.; Koga, O. *Electrochim. Acta* **1994**, *39*, 1833−1839.
(27) Stalder, C. J.; Chao, S.; Wrighton, M. S. *J. Am. Chem. Soc.* **1984**, *106*, 3673−3675.
(28) Kang, P.; Zhang, S.; Meyer, T. J.; Brookhart, M. *Angew. Chem., Int. Ed.* **2014**, *53*, 8709−8713.
(29) Armstrong, F. A.; Hirst, J. *Proc. Natl. Acad. Sci. U. S. A.* **2011**, *108*, 14049−14054.

DOI: 10.1021/acscatal.5b00602
ACS Catal. 2015, 5, 3916−3923